

Nonhydrogenic Rydberg atoms in a magnetic field: A rigorous semiclassical approach

Bruno Hüpfer,¹ Jörg Main,² and Günter Wunner²

¹*Fachbereich Physik und Institut für Chemie und Biologie des Meeres,*

Carl von Ossietzky Universität, Postfach 2503, D-26111 Oldenburg, Germany

²*Institut für Theoretische Physik I, Ruhr-Universität Bochum, D-44780 Bochum, Germany*

(Received 10 August 1995)

Multielectron atoms in external fields are essentially more complicated than hydrogen with regard to theoretical treatments. Experimental spectra of helium as well as R -matrix quantum-defect calculations revealed discrepancies between the diamagnetic hydrogen atom and general Rydberg atoms. They appeared most transparent as novel resonance structures in constant scaled-energy recurrence spectra of nonhydrogenic atoms at positions where no hydrogenic resonances exist. To reveal the physical origin of these resonances we performed a rigorous semiclassical investigation of nonhydrogenic atoms in magnetic fields. The ionic core is introduced into the Hamiltonian via a short-ranged core potential. For this Hamiltonian we analyze in detail the classical dynamics of closed orbits. Classical core-scattering results in the creation of a huge number of new closed orbits. They appear to be composed of a sequence of slightly different hydrogenic orbits, interconnected by the core-scattering, and can be grouped into families accordingly. With a semiclassical closed-orbit theory generalized to arbitrary quantum defects of the ionic core and with the closed orbits at hand we are able to calculate photoabsorption spectra of nonhydrogenic atoms. Although each of the new orbits has a low amplitude, the interference of all members of a family results in clearly visible resonances in the Fourier transform recurrence spectra, in good agreement with experiment and quantum calculations. The novel structures in nonhydrogenic spectra are now identified and semiclassically interpreted in terms of families of core-scattered classical orbits.

PACS number(s): 32.60.+i, 03.65.Sq, 05.45.+b, 32.70.Cs

I. INTRODUCTION

Highly excited atoms in magnetic fields have been shown to be ideally suited — as real physical examples of nonintegrable systems — to study experimentally and theoretically the quantum manifestations of classical chaos [1–3]. Even the simplest system, the hydrogen atom, placed in a uniform magnetic field, is neither separable nor integrable in the regime where the magnetic and Coulomb force are of comparable strength, a condition fulfilled in atoms excited close to the ionization threshold [4]. The classical dynamics is chaotic, i.e., no invariant tori exist to calculate individual quantum states via semiclassical torus quantization. Nevertheless, since the discovery of quasi-Landau resonances in barium [5], it turned out that closed classical orbits are of special importance for modulations of the photoabsorption spectra. The quasi-Landau resonances could be interpreted semiclassically as a periodic motion of the electron in the plane perpendicular to the magnetic field axis [6]. In later experiments on hydrogen different types of quasi-Landau resonances were observed and explained in terms of closed orbits out of the plane perpendicular to the field [7]. The method of *constant scaled-energy spectroscopy* enables a systematic experimental search for the entirety of quasi-Landau resonances related to closed classical orbits [8].

The measurements were accompanied by extensive theoretical investigations. Most of the theoretical work has been restricted to the hydrogen atom, which served — because of its simplicity and fundamental importance — as a basis also for the understanding of nonhydrogenic atoms. Fundamental advance in a semiclassical description of the photo cross section in terms of classical orbits was achieved by a *closed-*

orbit theory [9,10]. The theory allows a quantitative calculation of recurrence spectra reproducing in detail the resonance structures experimentally observed in hydrogenic atoms [11] and even explains most of the structures in nonhydrogenic recurrence spectra, e.g., in helium [12].

Nevertheless, exact quantum-defect R -matrix calculations [13–15] and experimental investigations [14] reveal puzzling structures in recurrence spectra of general Rydberg atoms in magnetic fields; i.e., changes are observed in the intensities of resonances, and, most interesting, resonances appear at positions where no closed orbits exist in the hydrogen atom. Similar nonhydrogenic signatures have recently also been observed in experimental Stark spectra of lithium [16] and in spectra of rubidium atoms in crossed magnetic and electric fields [17]. As general Rydberg atoms differ from hydrogen in the existence of a non-Coulombic ionic core, a detailed analysis of core effects, and particular, of core-scattering is necessary to explain the nonhydrogenic resonance structures.

In a semiclassical approach Gao, Delos, and Baruch incorporated quantum defects into the *closed-orbit theory* and compared semiclassical and experimental Stark spectra of sodium in the positive energy regime [18]. In these spectra, core-scattering effects were unessential compared with the quality of the available experimental data and only hydrogenic orbits have been considered in their calculations. Obviously it is impossible to explain the nonhydrogenic resonance structures in Refs. [13–15] in this approximation.

Another approach followed the R -matrix picture: The region outside the ionic core is treated semiclassically with hydrogenic classical orbits but core effects are considered fully quantum mechanically, i.e., as a quantum scattering of waves [15]. The method is able to reproduce the resonance

structures, which are interpreted in [15] as effects “beyond periodic orbits.” With this statement the fundamental question arises as to whether or not these structures can be explained fully semiclassically in terms of different types of classical orbits.

The first completely semiclassical interpretation of nonhydrogenic spectra was given in Ref. [19], where the resonances were calculated with different types of classical core-scattered orbits. Briefly, the decisive start for the treatment of core effects in the framework of closed-orbit theory is the modeling of the ionic core by means of a suitable core potential and a consideration of this model potential with the classical movement of the highly excited electron. In this paper we report in detail the rigorous semiclassical investigation of general Rydberg atoms in magnetic fields.

The paper is organized as follows: In the next section we introduce the model core potential and discuss the classical scattering of orbits. In particular the classical deflection function is shown to be almost uniquely related to the quantum defects of the ionic core. In Sec. III we analyze the classical dynamics of the highly excited electron under the combined action of the Coulomb potential, the core, and the external magnetic field. In a systematic search we obtain new families of core-scattered closed orbits. In Sec. IV we derive the closed-orbit theory extended to arbitrary quantum defects. Finally, in Sec. V we apply the closed-orbit theory to the orbits of Sec. III. The semiclassically obtained recurrence spectra are compared with recent R -matrix quantum calculations and experimental measurements and reveal an interpretation of nonhydrogenic resonance structures in terms of classically core-scattered closed orbits.

II. MODEL CORE POTENTIAL FOR GENERAL RYDBERG ATOMS

The exact nonrelativistic Hamiltonian for an N -electron atom in a magnetic field of strength B directed along the z axis reads

$$H_{\text{exact}} = \sum_{i=1}^N \frac{\mathbf{p}_i^2}{2m} - \sum_{i=1}^N \frac{Ze^2}{4\pi\epsilon_0 r_i} + \sum_{i<j} \frac{e^2}{4\pi\epsilon_0 |\mathbf{r}_i - \mathbf{r}_j|} + \sum_{i=1}^N \left(\frac{e}{2m} B L_{z,i} + \frac{e^2}{8m} B^2 \rho_i^2 \right). \quad (1)$$

We are dealing with Rydberg atoms where only one electron is highly excited close to the ionization threshold but the ionic core remains in the ground state. In this situation the nuclear charge is screened by the inner electrons and the complexity of the exact problem can be substantially simplified to the movement of the highly excited electron in an attractive Coulomb potential modified by a short-ranged core potential combined with an external magnetic field directed along the z axis. In atomic units [with $\gamma = B/(2.35 \times 10^5 \text{ T})$ the magnetic field strength] the Hamiltonian of the highly excited electron reads

$$H = \frac{1}{2} \mathbf{p}^2 + \frac{1}{2} \gamma L_z + \frac{1}{8} \gamma^2 \rho^2 + V(r). \quad (2)$$

The potential $V(r)$ of the nucleus and the core is assumed to be spherical symmetric and must comply with the two conditions

$$V(r) \xrightarrow{r \rightarrow 0} -\frac{Z}{r} \quad \text{and} \quad V(r) \xrightarrow{r \rightarrow \infty} -\frac{1}{r}$$

natural to general Rydberg atoms. Instead of performing Hartree-Fock calculations we use an analytical form that allows an easy integration of classical trajectories. Anyway, our intention is not to describe one particular atom to the greatest accuracy but to study the general effects of an additional short-ranged potential on the photoabsorption spectra. In order to have a simple dependence of the first derivative with respect to r we assume the following dependence on r :

$$V(r) = V_{\text{Coulomb}}(r) + V_{\text{core}}(r) = -\frac{1}{r} - \frac{Z-1}{r} \left(1 + \frac{r}{a} \right) e^{-r/a}, \quad (3)$$

where Z is the nuclear charge and a is a free length parameter determining the range of the core. This kind of potential has also been used in recent studies of nonhydrogenic atoms [20].

In comparison with hydrogen, the classical equations of motion derived from the Hamiltonian (2) are now modified by the presence of a short-ranged core potential in (3). In the following we discuss the changes of classical trajectories in the vicinity of the core, in particular the deflection of core-scattered orbits. The complete classical dynamics including the external magnetic field is analyzed in Sec. III.

In quantum mechanics the ionic core is entirely characterized by quantum defects μ_ℓ , or for energies $E > 0$ by phase shifts δ_ℓ . At the ionization threshold, these two quantities are connected by Seaton's theorem

$$\delta_\ell = \pi \mu_\ell.$$

The quantum defects can be calculated from the core potential (3) (see Appendix A) and depend in this model on the nuclear charge Z , the length a , and the azimuthal quantum number ℓ . For increasing ℓ the quantum defects become rapidly small, whereas they ascend with growing Z or a .

Classically, the core potential leads to a deflection of a trajectory incident with impact parameter b , which is directly related to the classical angular momentum $L = (\ell + 1/2)\hbar$. The classical scattering is most easily described in semiparabolic coordinates (see Appendix B), where purely Coulombic orbits at energy $E = 0$ are simply straight lines. If an additional attractive core is considered trajectories are deflected as shown in Fig. 1. For $b = L = 0$ no core scattering takes place, whereas with increasing L the trajectories are more and more deflected, until the deflection angle reaches a maximum. With further growing impact parameter the deflection angle decreases until finally the electron moves outside the region of the short-ranged core potential. The deflection function $\Theta(\ell)$ for different kinds and parameters of the core potential (3) is shown in Fig. 2. Our model potential causes no singularities in $\Theta(\ell)$; i.e., trajectories are not trapped by the core. The model potential (3) has to be chosen in such a way that the resulting quantum defects approximate those of the investigated atom.

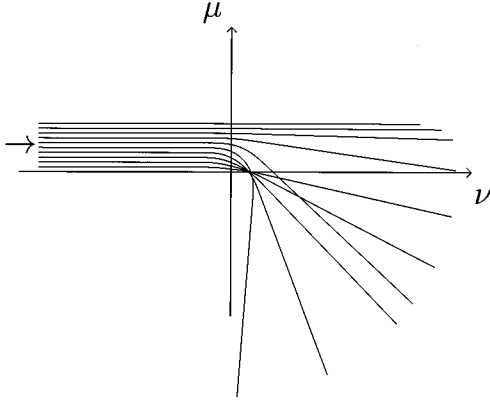


FIG. 1. Classical scattering of trajectories at the ionic core (in semiparabolical coordinates; energy $E=0$). Nonscattered Coulombic orbits are straight lines.

Some remarks are necessary about the arbitrariness of the choice of the core potential, as the classical dynamics and the creation of new types of orbits discussed in Sec. III depends sensitively on this choice. Quantum mechanically the ionic core is entirely described by the quantum defects. But there exists an almost unique relation between the quantum defects and the asymptotic behavior of the classical core scattering, i.e., the deflection function $\Theta(\ell)$. To show this we calculate the classical deflection function $\Theta(\ell)$ and the semiclassical quantum defects μ_ℓ for an arbitrary core potential (3). The deflection angle, i.e., the difference between the polar angles of the incoming and outgoing electron as a function of ℓ (at energy $E \approx 0$ around the ionization threshold) is obtained from classical mechanics [21]:

$$\Theta(\ell) = \sqrt{2} \int_{r_{0,c}}^{\infty} \frac{(\ell + 1/2) dr}{r^2 \sqrt{1/r - (\ell + 1/2)^2 / 2r^2}} - \sqrt{2} \int_{r_{0,c}}^{\infty} \frac{(\ell + 1/2) dr}{r^2 \sqrt{-V(r) - (\ell + 1/2)^2 / 2r^2}}, \quad (4)$$

with $V(r)$ the core modified Coulomb potential (3) and $r_{0,c}$ and r_0 the classical turning points depending on ℓ . The quantum defects μ_ℓ are semiclassically given as the difference in actions

$$\mu_\ell = \frac{\sqrt{2}}{\pi} \lim_{R \rightarrow \infty} \left[\int_{r_{0,c}}^R \sqrt{-V(r) - \frac{(\ell + 1/2)^2}{2r^2}} dr - \int_{r_0}^R \sqrt{\frac{1}{r} - \frac{(\ell + 1/2)^2}{2r^2}} dr \right]. \quad (5)$$

Applying the formula

$$\frac{d}{dy} \int_{x_1(y)}^{x_2(y)} f(x, y) dx = \int_{x_1(y)}^{x_2(y)} \frac{\partial f(x, y)}{\partial y} dx + f(x_2, y) \frac{dx_2}{dy} - f(x_1, y) \frac{dx_1}{dy}$$

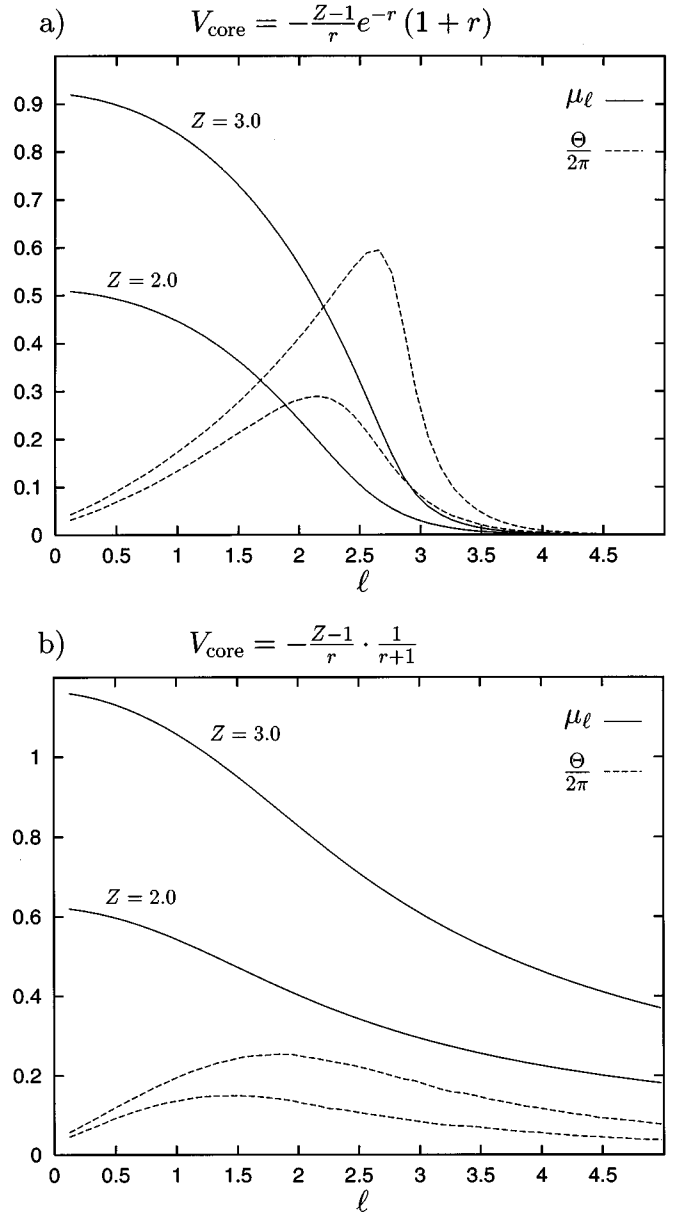


FIG. 2. Quantum defect μ_ℓ and classical deflection function $\Theta(\ell)/2\pi = d\mu_\ell/d\ell$ for two different kinds of core potentials. (a) Core potential of Eq. (3) with $a=1$. (b) Core potential $V_{\text{core}}(r) = -(Z-1)/r(r+1)$.

to the calculation of the derivative of μ_ℓ with respect to ℓ and comparing the result with the classical deflection function $\Theta(\ell)$ we finally obtain the very general relation

$$\Theta(\ell) = 2\pi \frac{d\mu_\ell}{d\ell} \quad (6)$$

between the quantum defects and the deflection function. It is illustrated in Fig. 2 for two different examples of model potentials. Consequently, if the quantum defects μ_ℓ for $\ell=0,1,2,\dots$ are fixed, the maximum deflection angle, Θ_{max} is determined, as well, independent of the special form of the core potential, provided that μ_ℓ does not fluctuate too much with changing ℓ . The maximum deflection angle is directly related to the creation of core-scattered closed orbits:

Only those nonhydrogenic orbits exist whose deflection angle between interlinked hydrogenic orbits is less than Θ_{\max} . Equation (6) ensures that the classical dynamics of nonhydrogenic atoms analyzed in the next section is almost uniquely related to the quantum defects of the investigated atom provided the model potential is adjusted to these quantum defects. The classical dynamics does not depend sensitively on a special analytical choice of the core potential.

III. CREATION OF NEW CLOSED ORBITS THROUGH CLASSICAL CORE SCATTERING

Here we examine the classical dynamics of the highly excited electron in the core modified Coulomb potential (3) combined with an external magnetic field. The equations of motion obtained from the total Hamiltonian (2) are regularized in semiparabolical coordinates and integrated numerically (see Appendix B). As in the hydrogenic case, where it is well known that closed orbits starting at and returning to the nucleus produce modulations in the photo cross section [11], we expect to explain the structures in nonhydrogenic recurrence spectra in terms of closed orbits as well. Therefore we give special attention to the existence of different types of nonhydrogenic closed orbits.

Indeed, scattering by the core potential leads to the creation of a huge number of periodic orbits. With the knowledge about core scattering from the previous section a first understanding of the shape of the orbits can be obtained. A trajectory starting in almost the same initial direction as a hydrogenic closed orbit leaves the nucleus radially and evolves hydrogenlike outside the region of the ionic core. As the orbit returns to the nucleus it is scattered by the core potential. There are two possible ways for the nonhydrogenic orbit to go: It can pass the core potential by leaving the nucleus either on its right or on its left side. Two examples are given with orbits (a) and (b) in Fig. 3 where the core region is expanded separately to elucidate the scattering. The electron is deflected and, contrary to hydrogen, the direction of the outgoing electron does not agree with the incoming direction but may now almost agree with the initial direction of another hydrogenic closed orbit. Furthermore for each scattering angle there exist two values for the impact parameter leading to two slightly different orbits, as illustrated in Figs. 3(c) and 3(d). Outside the ionic core the electron again evolves hydrogenlike and may then be scattered a second time, a third time, etc. until finally it returns to the nucleus exactly where the orbit is closed. Thus the nonhydrogenic closed orbits appear to be composed of two or more hydrogenic orbits. The greater the maximal scattering angle, Θ_{\max} , the greater the number of possible interconnections of hydrogenic orbits. This illuminates a huge and rapid increase in the number of multiple scattered closed orbits. The nonhydrogenic orbits are created with increasing maximum deflection angle via a cascade of bifurcations. It would be interesting to study the bifurcation scheme in detail and to observe the occurrence of nonhydrogenic orbits in quantum mechanical and semiclassical spectra with increasing Θ_{\max} . This analysis is currently under investigation.

Because the complete knowledge of closed orbits up to a certain maximal length are the essential key to a semiclassical calculation of recurrence spectra we now perform a sys-

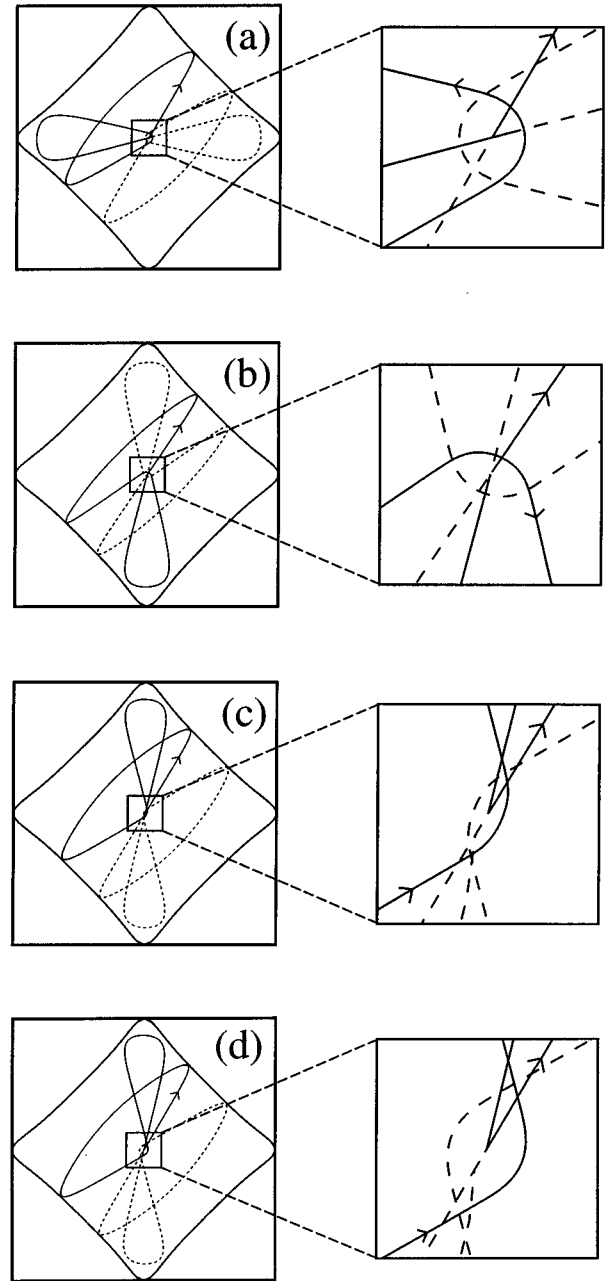


FIG. 3. Four examples of slightly different core-scattered orbits belonging to the same family $R_2^1 \oplus V_1^1$. Orbits (a) and (b) pass the nucleus on different sides, whereas orbits (c) and (d) differ only in their impact parameters. The full lines represent one and the dashed lines a second cycle of the orbits. The magnified sections elucidate in detail the scattering in the core region.

tematic search for both hydrogenic and core-scattered nonhydrogenic closed orbits. The scheme for this search becomes most transparent with the help of the following (S, ϑ) diagrams (see Fig. 4 and Fig. 5): Let a trajectory start at the origin with initial angle ϑ_i relative to the z axis. Whenever the orbit passes either the positive or negative z axis, i.e., $\rho=0$, its classical action $S = \int \mathbf{p}^2 dt$ is recorded in the (S, ϑ) diagram. Varying the starting angle ϑ_i the diagram exhibits lines belonging to orbital crossings of the positive and negative z axis, respectively. Now each closed orbit is

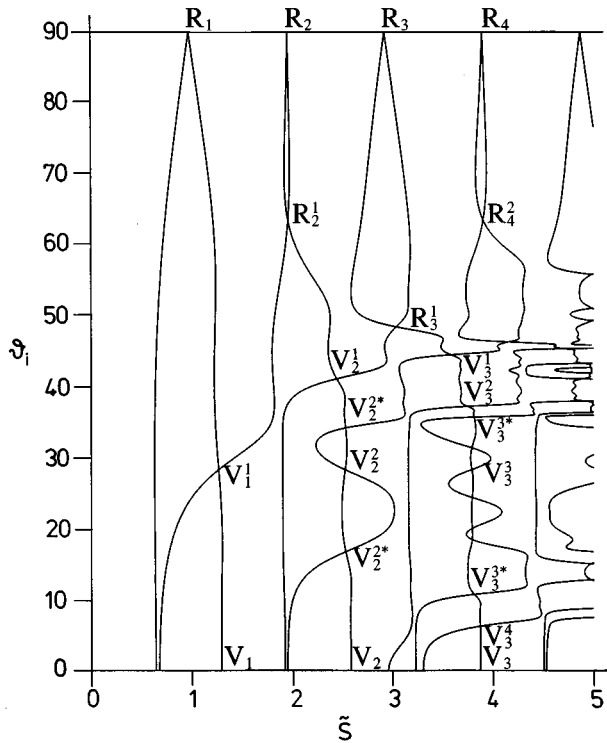


FIG. 4. (\tilde{S}, ϑ) diagram for the hydrogen atom at scaled energy $\tilde{E} = -0.3$. Lines correspond to trajectories passing either the positive or negative z axis. Crossings of lines indicate closed orbits, labeled in the nomenclature of Ref. [8].

obviously characterized by a simultaneous return of the electron to the positive and negative z axis, i.e., by a crossing of two lines in the (\tilde{S}, ϑ) diagram. Thus the starting angles and classical actions of all closed orbits can be directly obtained from the (\tilde{S}, ϑ) diagram as the crossings of two different lines. Figures 4 and 5 represent two examples of (\tilde{S}, ϑ) diagrams calculated at scaled energy $\tilde{E} = E\gamma^{-2/3} = -0.3$, Fig. 4 for the hydrogen atom and Fig. 5 for a nonhydrogenic atom with quantum defect $\mu_1 = 0.5$. A comparison illustrates a rapid increase in the number of closed orbits from 35 hydrogenic orbits in Fig. 4 to about 2600 core-scattered orbits in Fig. 5. The nonhydrogenic orbits are clustered at starting angles around those of hydrogenic orbits and the actions of these clusters are approximately the sum of two or more actions of hydrogenic orbits. If one has a closer look at them in coordinate space and does not consider in detail small differences in the core region, it turns out that they can be grouped into families of structurally similar orbits. As mentioned before, they seem to be composed of hydrogenic orbits interlinked by the scattering at the core and it is natural to introduce the following notation for the families: We write $h_1 \oplus h_2 \oplus h_3 \oplus \dots$ where h_i denotes the name of a primitive hydrogenic orbit and \oplus indicates the scattering at the core potential. For the hydrogenic orbits, h_i , we use the same nomenclature as in Ref. [8], i.e., orbits R_μ^ν are bifurcated from the motion perpendicular to the field axis, V_μ^ν denotes orbits directly bifurcated from the motion parallel to the field, and higher-order bifurcations are marked by an asterisk. For example, the orbits in Fig. 3 belong to the family $R_2^1 \oplus V_1^1$.

Because the classical action of nonhydrogenic orbits is

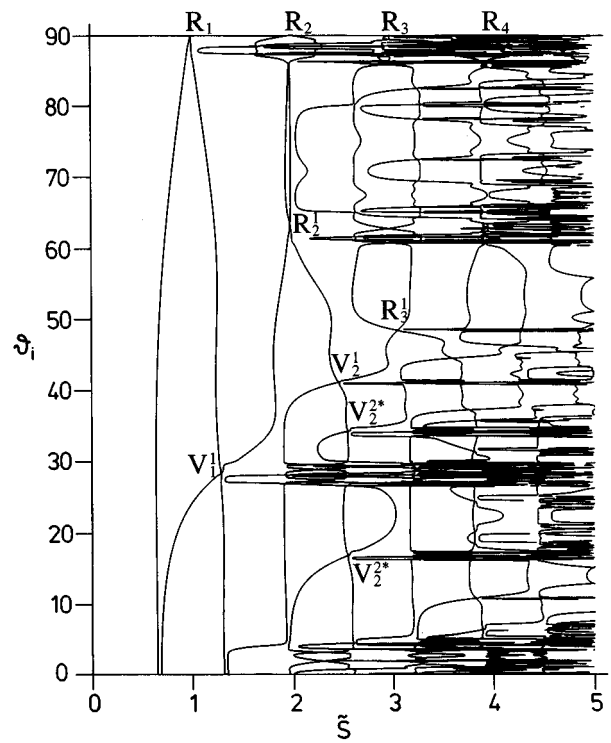


FIG. 5. Same as Fig. 4 but for a nonhydrogenic atom with quantum defect $\mu_1 = 0.5$. The rapid increase in the number of nonhydrogenic closed orbits is clearly exhibited.

almost the sum of hydrogenic ones they may be clustered at recurrence positions where a hydrogenic orbit does not necessarily exist. For example, in Fig. 5 clusters of orbits exist between $\tilde{S} \approx 4.2$ and $\tilde{S} \approx 4.6$, i.e., at positions where novel resonance structures have been discovered in R -matrix quantum calculations [13]. In this way the new resonances, which have recently been discovered in nonhydrogenic atoms [13,14,16] can already *qualitatively* be explained by clusters of core-scattered closed classical orbits. A complete *quantitative* comparison of recurrence spectra will be possible with the help of a closed-orbit theory extended to general Rydberg atoms in the next paragraph.

IV. CLOSED-ORBIT THEORY EXTENDED TO NONHYDROGENIC ATOMS

Here, we present the closed-orbit theory of general Rydberg atoms in magnetic fields with a complete consideration of core effects via quantum defects and classical core scattering. The closed-orbit theory has been originally developed for the hydrogen atom in a magnetic field by Du and Delos [9] and Bogomolny [10] and has been extended to incorporate quantum defects by Gao, Delos, and Baruch [18]. For completeness we report the physical picture and the derivation of semiclassical formulas. Although we tried to shorten the derivations as much as possible, the theory is quite lengthy. The final results are to be found with Eq. (36), where the oscillator strength is expressed in terms of all closed classical orbits, and with Eq. (42) for the scaled recurrence spectra.

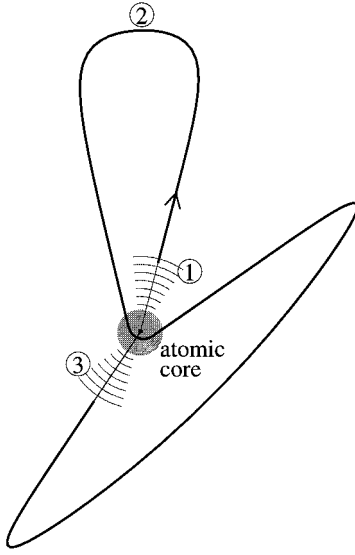


FIG. 6. Sketch of the semiclassical excitation mechanism (see text): (1) A radially outgoing Coulomb wave is produced by photoabsorption. (2) The wave is propagated semiclassically along classical trajectories that are eventually scattered several times at the ionic core. (drawn is a single-scattered orbit.) (3) Finally returning orbits are joined to incoming Coulomb waves.

A. Physical picture

The semiclassical excitation mechanism can be roughly divided into three different steps sketched in Fig. 6.

(1) A state initially located close to the nucleus is excited by a photon creating an outgoing Coulomb wave which is phase shifted in the case of nonhydrogenic atoms with respect to the quantum defects of the ionic core.

(2) The further propagation of this wave is regarded semiclassically along classical trajectories according to the full Hamiltonian (2), i.e., including core scattering of returning orbits (see Fig. 6). In this step the physical picture differs substantially from Ref. [15] where a semiclassical propagation is restricted to regions out of core and core effects are treated as quantum scattering.

(3) The finally returning trajectories are joined to incoming Coulomb waves and the interference of incoming and outgoing waves create modulations in the oscillator strength.

Going into detail, we start with the exact quantum expression for the oscillator strength for dipole transitions of an initial state Ψ_i to final states at energy E

$$f(E) = -\frac{2}{\pi}(E - E_i) \text{Im} \int d^3x (\mathbf{D}\Psi_i)^*(\mathbf{x}) \mathcal{F}(\mathbf{x}), \quad (7)$$

where D is the dipole operator and $\mathcal{F}(\mathbf{x})$ the solution of the inhomogeneous Schrödinger equation

$$[E - \hat{H} + i\varepsilon] \mathcal{F}(\mathbf{x}) = (\mathbf{D}\Psi_i)(\mathbf{x}). \quad (8)$$

The quantum wave $\mathcal{F}(\mathbf{x})$ can be semiclassically approximated as explained in the following. The initial state is located close to the nucleus (within a few Bohr radii, whereas

the final state is usually extended over several thousand Bohr radii). In order to compute the integral in (7) it is sufficient to know $\mathcal{F}(\mathbf{x})$ in the vicinity of the nucleus, where the magnetic field is negligible compared with the Coulomb force and special solutions of the inhomogeneous Schrödinger equation (8) are outgoing Coulomb waves. On account of the short-ranged core potential, the waves own an additional phase shift $\delta_\ell = \pi\mu_\ell$. The outgoing Coulomb wave is calculated in Sec. IV B.

In the outer region the magnetic field must no longer be neglected and the wave function is now propagated semiclassically along classical trajectories. These trajectories, which are directed radially at first, then feel the additional Lorentz force and show up signatures of classical chaos. They evolve according to the Hamiltonian equations, where the full core potential is used. Eventually they are scattered at the atomic core. The amplitude of the semiclassical wave function at a given point (r, ϑ) depends on the stability properties of the trajectories reaching (r, ϑ) and its phase is related to the classical action S and the number α of conjugate points, i.e., the Maslov index. The semiclassical wave is constructed in Sec. IV C.

When the trajectory finally returns to the nucleus the wave function is joined to Coulomb scattering waves (see Sec. IV D) and after separating the φ dependence the following ansatz of $\mathcal{F}(\mathbf{x})$ as a superposition of an outgoing and returning waves is valid close to the origin:

$$\mathcal{F}(\mathbf{x}) = \sum_m [\Psi_m^{\text{out}}(r, \vartheta) + \Psi_m^{\text{ret}}(r, \vartheta)] e^{im\varphi}. \quad (9)$$

The incoming and outgoing waves interfere and produce oscillations in the photo cross section. With the wave function (9) at hand the semiclassical oscillator strength (7) is obtained in Sec. IV E.

B. Outgoing Coulomb waves

Close to the nucleus where the magnetic field can be neglected the inhomogeneous Schrödinger equation (8) for the Hamilton operator

$$\hat{H} = \frac{1}{2} \hat{\mathbf{p}}^2 - \frac{1}{r} + V_{\text{core}} \quad (10)$$

is solved with the help of the Green's function expanded in spherical harmonics

$$\mathcal{G}^+(\mathbf{x}, \mathbf{x}') = \sum_{\ell m} Y_{\ell m}^*(\vartheta', \varphi') g_{\ell}^E(r, r') Y_{\ell m}(\vartheta, \varphi)$$

and the outgoing waves can be written as

$$\Psi_m^{\text{out}}(r, \vartheta) = \sum_{\ell=|m|}^{\infty} \int d\mathbf{x}' Y_{\ell m}^*(\vartheta', \varphi') g_{\ell}^{E=0}(r, r') Y_{\ell m}(\vartheta, \varphi) \times (\mathbf{D}\Psi_i)(\mathbf{x}'). \quad (11)$$

Here we took $g_{\ell}^{E=0}$, an approximation valid for small r and for states highly excited close to the ionization threshold. The radial Green's function is gained from a regular and an irregular solution [22]

$$g_{\ell}^0(r, r') = \frac{2R_{\ell}^{0,\text{reg}}(r_{<})R_{\ell}^{0,\text{out}}(r_{>})}{r'^2 \mathcal{W}[R_{\ell}^{0,\text{reg}}(r'), R_{\ell}^{0,\text{out}}(r')]},$$

where $r_{<} = \min\{r, r'\}$, $r_{>} = \max\{r, r'\}$ and with $\mathcal{W}(f_1, f_2) = f_1 f_2' - f_1' f_2$ the Wronskian determinant. For hydrogen the regular and irregular solutions consist of Bessel and Neumann functions, respectively, whereas for nonhydrogenic atoms they can be written down in the asymptotic region as a linear combination of hydrogenic solutions, with prefactors depending on the phase shifts:

$$R_{\ell}^{0,\text{reg}}(r) \xrightarrow{r > r_{\text{core}}} \sqrt{\frac{2}{r}} [\cos \delta_{\ell} J_{2\ell+1}(\sqrt{8r}) - \sin \delta_{\ell} N_{2\ell+1}(\sqrt{8r})], \quad (12)$$

$$R_{\ell}^{0,\text{irr}}(r) \xrightarrow{r > r_{\text{core}}} \sqrt{\frac{2}{r}} [\cos \delta_{\ell} N_{2\ell+1}(\sqrt{8r}) + \sin \delta_{\ell} J_{2\ell+1}(\sqrt{8r})]. \quad (13)$$

In the outgoing radial function the ionic core causes a phase shift δ_{ℓ} at distances $r > r_{\text{core}}$:

$$R_{\ell}^{0,\text{out}}(r) = R_{\ell}^{0,\text{reg}}(r) + iR_{\ell}^{0,\text{irr}}(r) = e^{i\delta_{\ell}} \sqrt{\frac{2}{r}} H_{2\ell+1}^{(1)}(\sqrt{8r}). \quad (14)$$

($H_n^{(1)} = J_n + iN_n$ is the Hankel function of the first kind.) Finally the outgoing wave can be written down:

$$\Psi_m^{\text{out}}(r, \vartheta) = -\pi i \sum_{\ell=|m|}^{\infty} R_{\ell}^{0,\text{out}}(r) Y_{\ell m}(\vartheta, \varphi) \underbrace{\int d^3x' (\mathbf{D}\Psi_i)(x') R_{\ell}^{0,\text{reg}}(r') Y_{\ell m}^*(\vartheta', \varphi')}_{B_{\ell m}} \quad (15)$$

The coefficients $B_{\ell m}$ depend only on the dipole operator and on the initial state. As we do not know the initial wave function inside the core region ($r < r_{\text{core}}$), they are unknown, but constant. Only in the hydrogenic case can they be calculated analytically. For the dipole transition considered here they lead to a constant factor in the spectra. Together with an asymptotic property of the Hankel function

$$H_n^{(1)}(x) \xrightarrow{x \rightarrow \infty} \sqrt{\frac{2}{\pi x}} e^{i[x - \pi/2n - \pi/4]}$$

one obtains the asymptotic form of the outgoing wave:

$$\Psi_m^{\text{out,as}}(r, \vartheta) = -\sqrt{\pi} 2^{1/4} r^{-3/4} e^{i(\sqrt{8r} - \pi/4)} \underbrace{\sum_{\ell=|m|}^{\infty} (-1)^{\ell} e^{i\delta_{\ell}} B_{\ell m} Y_{\ell m}(\vartheta, 0)}_{y_m^{\delta}(\vartheta)} \quad (16)$$

The angular functions $y_m^{\delta}(\vartheta)$ depend on the initial state, the dipole operator, and the quantum defects δ_{ℓ} of the ionic core.

C. Semiclassical propagation

When the outgoing waves reach a radius $r_i > r_{\text{core}}$, where a semiclassical approximation becomes valid but the magnetic term is still small enough compared with the Coulomb term, we proceed as follows: From now on we propagate the wave function semiclassically along classical trajectories in the combined fields. We follow the construction of Maslov and Fedoriuk [23], which is also described in Ref. [24]: Starting from an initial surface Σ^0 and integrating the classical action $S(q)$ and the density $\rho(q)$ along the solutions of Hamilton's equations, one can construct an asymptotic, i.e., correct in first order of \hbar , solution to Schrödinger's equation:

$$\Psi(q) = \sqrt{\rho(q)} e^{iS(q)/\hbar}. \quad (17)$$

Every orbit starting on the initial surface Σ^0 and passing through q gives a contribution to $\psi(q)$ of the form (17). The density $\rho(q)$ depends on the divergence of adjacent trajectories:

$$\rho(q) = \frac{J(t=0, q^0)}{J(t, q^0)} \rho(q^0) \quad (18)$$

with the Jacobian

$$J(t, q^0) = \det \left| \frac{\partial(t, q^0)}{\partial(t, q)} \right|. \quad (19)$$

The action is defined as

$$S(q) = S(q^0) + \int_{q^0}^q p dq. \quad (20)$$

For the systems considered here, i.e., atoms in external fields, the wave function on the initial sphere with radius $r = r_i$ is given by Eq. (16) and may be written as

$$\Psi_m(r_i, \vartheta) = \sqrt{\rho_m(r_i, \vartheta)} e^{i[S(r_i) - \pi/4]}, \quad (21)$$

with

$$\sqrt{\rho_m(r_i, \vartheta)} = -\sqrt{\pi} 2^{1/4} r_i^{-3/4} \mathcal{J}_m^\delta(\vartheta) \quad (22)$$

the density of classical trajectories, and

$$S(r_i) = \sqrt{8} r_i = \int_0^{r_i} \sqrt{2/r} dr \quad (23)$$

the action of a classical trajectory starting at the nucleus and propagated to $r = r_i$ in a pure Coulomb field, i.e., *without* consideration of the core potential. The formulas suggest to start formally all trajectories at the origin and on the condition that we have to “switch off” the core potential in the beginning in order to neglect core effects that are already incorporated in the $\mathcal{J}_m^\delta(\vartheta)$ in (22). Then, a correct calculation of the stability properties is guaranteed as well.

The outgoing wave propagates along classical trajectories starting with angle ϑ_i relative to the magnetic field axes. The trajectories are those of an electron experiencing the Coulomb force plus the short-ranged core potential and the Lorentz force. Each trajectory, labeled with the index k , gives at (r, ϑ) a contribution of the form

$$\Psi_{m,k}^{\text{semi}}(r, \vartheta) = \sqrt{J(t_i, \vartheta_{i,k})/|J(t, \vartheta_{i,k})|} \sqrt{\rho_{m,k}(r_i, \vartheta_{i,k})} \times e^{i[S_{m,k}(r, \vartheta) - (\pi/2)\alpha_k + \pi/4]}, \quad (24)$$

where $S_{m,k}(r, \vartheta)$ denotes the action of an electron starting at the origin (with the core potential switched off at the beginning). It is divided into two parts:

$$S_{m,k} = S_k + m\left(\frac{1}{2}\gamma T_k + \pi n_{z,k}\right), \quad (25)$$

where S_k is the action for magnetic quantum number $m = 0$, i.e., the action of the (r, ϑ) motion, whereas the second term approximates the action of the separated ϕ motion. T_k is the recurrence time and the index $n_{z,k}$ is incremented by one every time the orbit touches the z axes and, moreover, it is incremented by one at the start and at the end and incremented by two every time the orbit passes the origin. The Maslov index α_k increases by one every time the trajectory passes a conjugate point or a caustic, where the Jacobian $J(t, \vartheta_i)$ vanishes, and is incremented additionally by one at the beginning and the end of the trajectory. The Jacobian

$$J(t, \vartheta_i) = \det \left| \frac{\partial(x, y, z)}{\partial(t, \vartheta_i, \varphi)} \right| = r^2 \sin \vartheta \det \left| \frac{\partial(r, \vartheta)}{\partial(t, \vartheta_i)} \right| \quad (26)$$

is given on the initial sphere (close to the nucleus where $B \approx 0$ and $E \approx 0$) for radially outgoing trajectories as

$$J(t_i, \vartheta_{i,k}) = \sqrt{2} \sin \vartheta_{i,k} r_i^{3/2}.$$

The semiclassical wave function at (r, ϑ) now reads

$$\Psi_m^{\text{semi}}(r, \vartheta) = -\sqrt{2\pi} \sum_k \sqrt{\sin \vartheta_{i,k}/r^2 \sin \vartheta \det |\partial(r, \vartheta)/\partial(t, \vartheta_i)|} \times \mathcal{J}_m^\delta(\vartheta_{i,k}) e^{i[S_{m,k}(r, \vartheta) - (\pi/2)\alpha_k + (\pi/4)]}. \quad (27)$$

Concerning the applicability of the semiclassical approximation it may be noted that for highly excited atoms at laboratory field strength the configuration-space form of the semiclassical condition is valid in the classically allowed region except (a) close to its border where the classical momentum becomes extremely small and (b) close to the origin where the potential is singular. In case of (a) a momentum-space form of the semiclassical approximation is appropriate [9]. In region (b), i.e., close and inside the ionic core the applicability of the semiclassical approximation is not at all obvious and a further discussion is necessary: For the model potential (3) we calculated the partial radial wave functions $R_{\ell}^{\text{reg}}(r)$ quantum mechanically via numerical integration of Schrödinger's equation and semiclassically. A comparison of the quantum defects μ_{ℓ} (see Appendix A) demonstrates a good agreement in the asymptotic wave functions. Therefore we finally conclude that the semiclassical approximation is appropriate for the problem as a whole, provided the Maslov index is considered correctly.

D. Finally returning waves

In Eq. (27) the semiclassical wave function has to be calculated in an implicit way. Moreover, it is not valid close to the origin where the semiclassical condition breaks down. On the other hand the calculation of oscillator strength via Eq. (7) requires the explicit knowledge of returning waves close to the origin. For this purpose the semiclassical waves of finally returning classical trajectories are joined to incoming Coulomb scattered waves as described in the following text.

In Eq. (27) the action $S_{m,k}(r, \vartheta)$ of an almost closed orbit k incoming at the angle $\vartheta_{f,k}$ is approximated in the vicinity of the nucleus (but $r > R_{\text{core}}$) by

$$S_{m,k}(r, \vartheta) = S_{m,k}^0 - \sqrt{8}r + \sqrt{\frac{r}{8}}(\vartheta - \vartheta_{f,k})^2 + \frac{\pi}{2} \quad (28)$$

(see Appendix C), where $S_{m,k}^0$ is the action of the orbit exactly returning to the origin but without consideration of the core potential at the final return, i.e., the same rule for the “switching off” holds for the initial start and final return of a closed trajectory. The additional phase of $+\pi/2$ in (28) is necessary for a correct counting of the Maslov index consistent with the definition that α_k is incremented by one at the final return of a closed orbit.

The determinant in (27) can be expressed by one element of the monodromy matrix M computed in semiparabolical coordinates (see Appendix D):

$$\det \left| \frac{\partial(r, \vartheta)}{\partial(t, \vartheta_i)} \right| = \frac{2}{r} m_{12,k}. \quad (29)$$

The monodromy matrix M_k is nearly independent of r close to the nucleus but outside the ionic core ($r > r_{\text{core}}$), i.e., in the region where the semiclassical returning wave has to be joined to an incoming Coulomb scattered quantum wave. It is therefore quite natural to calculate the monodromy matrix of a closed orbit on the condition that the core potential is “switched off” at the start and final return. By means of this procedure, the Liapunov exponents of primitive orbits not scattered at the core (and consequently the amplitudes of returning waves) are the same for hydrogenic and nonhydrogenic atoms. It may be noted that the Liapunov exponents of closed orbits defined and computed in this way differ from those obtained in [20] where the core potential is considered to include the start and final return of trajectories. The stability coefficients of Ref. [20] are not suitable to be used in the semiclassical theory.

Inserting the above expressions in Eq. (27) we obtain the incoming semiclassical wave function in the vicinity of the nucleus as a sum over all trajectories closed at the nucleus:

$$\begin{aligned} \Psi_m^{\text{in,semi}}(r, \vartheta) &= -\sqrt{\pi} \sum_{\text{cl.o.k}} \sqrt{\sin \vartheta_{i,k} / r \sin \vartheta |m_{12,k}|} \mathcal{Y}_m^\delta(\vartheta_{i,k}) \\ &\times e^{i[S_{m,k}^0 - (\pi/2)\alpha_k + (\pi/4)]} \\ &\times e^{-i[\sqrt{8r} - \sqrt{r/8}(\vartheta - \vartheta_{f,k})^2 - (\pi/2)]}. \end{aligned} \quad (30)$$

The exact quantum mechanical stationary state of the core-scattered waves is a superposition of an incoming wave $\sqrt{2/r} H_{2\ell+1}^{(2)}(\sqrt{8r})$ and an outgoing wave $\sqrt{2/r} H_{2\ell+1}^{(1)}(\sqrt{8r})$ with prefactors including a total phase shift of $2\delta_\ell$ between the two waves due to the core potential:

$$\begin{aligned} \Psi_{\ell}^{\text{scat}}(r) &\xrightarrow{r > r_{\text{core}}} \sqrt{\frac{2}{r}} [H_{2\ell+1}^{(2)}(\sqrt{8r}) + e^{2i\delta_\ell} H_{2\ell+1}^{(1)}(\sqrt{8r})] \\ &= e^{i\delta_\ell} R_{\ell}^{0,\text{reg}}(r). \end{aligned} \quad (31)$$

Now, in the asymptotic limes $r > r_{\text{core}}$, we expand the returning wave function Ψ_m^{ret} , needed in Eq. (9), in terms of the Coulomb scattered wave functions and spherical harmonics:

$$\begin{aligned} \Psi_m^{\text{ret}}(r, \vartheta) &= \sum_{\ell=|m|}^{\infty} c_{\ell m} \Psi_{\ell}^{\text{scat}}(r) Y_{\ell m}(\vartheta, 0) \\ &= \underbrace{\sum_{\ell=|m|}^{\infty} c_{\ell m} \sqrt{\frac{2}{r}} H_{2\ell+1}^{(2)}(\sqrt{8r}) Y_{\ell m}(\vartheta, 0)}_{\text{incoming wave}} + \underbrace{\sum_{\ell=|m|}^{\infty} c_{\ell m} \sqrt{\frac{2}{r}} e^{2i\delta_\ell} H_{2\ell+1}^{(1)}(\sqrt{8r}) Y_{\ell m}(\vartheta, 0)}_{\text{outgoing wave}} \end{aligned} \quad (32)$$

In order to determine the coefficients $c_{\ell m}$ we must compare the incoming part of the Coulomb scattered wave function (32) with the incoming semiclassical wave function (30). Using the orthogonality relation for the spherical harmonics we get

$$\begin{aligned} c_{\ell m} \sqrt{\frac{2}{r}} H_{2\ell+1}^{(2)}(\sqrt{8r}) &= 2\pi \int_0^\pi \Psi_m^{\text{in,semi}}(r, \vartheta) Y_{\ell m}(\vartheta, 0) \sin \vartheta d\vartheta \\ &= -(2\pi)^{3/2} \sum_{\text{cl.o.k}} \sqrt{\sin \vartheta_{i,k} / |m_{12,k}|} \mathcal{Y}_m^\delta(\vartheta_{i,k}) \sqrt{\frac{2}{r}} e^{i[S_{m,k}^0 - (\pi/2)\alpha_k + (\pi/4)]} \\ &\times \int_0^\pi e^{-i[\sqrt{8r} - \sqrt{r/8}(\vartheta_{f,k} - \vartheta)^2 - \pi/2]} \sqrt{\sin \vartheta} Y_{\ell m}(\vartheta, 0) d\vartheta. \end{aligned}$$

The integral is evaluated in the stationary phase approximation together with the assumption that $\sqrt{\sin \vartheta} Y_{\ell m}(\vartheta, 0)$ is nearly constant in the region of stationary phase, i.e., at $\vartheta \approx \vartheta_{f,k}$:

$$\begin{aligned} c_{\ell m} \sqrt{\frac{2}{r}} H_{2\ell+1}^{(2)}(\sqrt{8r}) &= -(2\pi)^{5/2} \sum_{\text{cl.o.k}} \sqrt{\sin \vartheta_{i,k} \sin \vartheta_{f,k} / |m_{12,k}|} \\ &\times (-1)^\ell \mathcal{Y}_m^\delta(\vartheta_{i,k}) Y_{\ell m}(\vartheta_{f,k}, 0) e^{i[S_{m,k}^0 - (\pi/2)\alpha_k + \pi/4]} \frac{2}{\sqrt{\pi}} (2r)^{-3/4} e^{-i[\sqrt{8r} - \pi l - (3/4)\pi]}. \end{aligned} \quad (33)$$

In the last term we recognize the asymptotic form of the radial incoming wave

$$\sqrt{\frac{2}{r}} H_{2\ell+1}^{(2)}(\sqrt{8r}) \xrightarrow{r \rightarrow \infty} \frac{2}{\sqrt{\pi}} (2r)^{-3/4} e^{-i[\sqrt{8r} - \pi l - (3/4)\pi]}$$

and finally obtain the coefficients

$$c_{\ell m} = -(2\pi)^{5/2} \sum_{\text{cl.o.k}} \sqrt{\sin\vartheta_{i,k} \sin\vartheta_{f,k}/|m_{12,k}|} (-1)^\ell \mathcal{Y}_m^\delta(\vartheta_{i,k}) Y_{\ell m}(\vartheta_{f,k}, 0) e^{i[S_{m,k}^0 - (\pi/2)\alpha_k + \pi/4]}, \quad (34)$$

which are inserted into (32) to get the returning wave function

$$\begin{aligned} \Psi_m^{\text{ret}}(r, \vartheta) = & -(2\pi)^{5/2} \sum_{\text{cl.o.k}} \sqrt{\sin\vartheta_{i,k} \sin\vartheta_{f,k}/|m_{12,k}|} \\ & \times \mathcal{Y}_m^\delta(\vartheta_{i,k}) e^{i[S_{m,k}^0 - (\pi/2)\alpha_k + \pi/4]} \sum_{\ell=|m|}^{\infty} (-1)^\ell e^{i\delta_\ell/R} R_{\ell}^{0,\text{reg}}(r) Y_{\ell m}(\vartheta_{f,k}, 0) Y_{\ell m}(\vartheta, 0). \end{aligned} \quad (35)$$

E. Oscillator strength

To obtain the semiclassical formula for the oscillator strength we now insert the expressions for the outgoing wave (15) and the returning wave (35) into Eq. (7). The integral in (7) results by analogy with (15) in coefficients $B_{\ell m}^*$ and the sum over ℓ quantum numbers in (35) can be reduced by analogy with (16) to functions

$$\tilde{\mathcal{Y}}_m^\delta(\vartheta) = \sum_{\ell=|m|}^{\infty} (-1)^\ell e^{i\delta_\ell} B_{\ell m}^* Y_{\ell m}(\vartheta, 0),$$

where the coefficients $B_{\ell m}$ are replaced by their complex conjugate, but the phase shifts due to the quantum defects ($e^{i\delta_\ell}$) keep their sign; i.e., the $\tilde{\mathcal{Y}}_m^\delta(\vartheta)$ in general differ from the complex conjugate of $\mathcal{Y}_m^\delta(\vartheta)$. As a final result we obtain the oscillator strength as the sum of a direct part from the dipole matrix element of Ψ_i with the outgoing wave Ψ_m^{out} , which produces a continuous background and contributions from all returning waves Ψ_m^{ret} which causes a superposition of oscillations in the spectrum:

$$f = f^0 + f^{\text{osc}} \quad (36)$$

with

$$\begin{aligned} f^0 = & 2(E_f - E_i) \sum_m |B_{\ell m}|^2, \\ f^{\text{osc}} = & 4(2\pi)^{3/2} (E_f - E_i) \text{Im} \left\{ \sum_{\text{cl.o.k}} \sqrt{\sin\vartheta_{i,k} \sin\vartheta_{f,k}/|m_{12,k}|} \right. \\ & \left. \times \sum_{m=-\infty}^{\infty} \mathcal{Y}_m^\delta(\vartheta_{i,k}) \tilde{\mathcal{Y}}_m^\delta(\vartheta_{f,k}) e^{i[S_{m,k}^0 - (\pi/2)\alpha_k + \pi/4]} \right\}, \end{aligned}$$

$$\mathcal{Y}_m^\delta(\vartheta) = \sum_{\ell=|m|}^{\infty} (-1)^\ell e^{i\delta_\ell} B_{\ell m} Y_{\ell m}(\vartheta, 0),$$

$$\tilde{\mathcal{Y}}_m^\delta(\vartheta) = \sum_{\ell=|m|}^{\infty} (-1)^\ell e^{i\delta_\ell} B_{\ell m}^* Y_{\ell m}(\vartheta, 0),$$

$$B_{\ell m} = \int d^3x (\mathbf{D}\Psi_i)(\mathbf{x}) R_{\ell}^{0,\text{reg}}(r) Y_{\ell m}^*(\vartheta, \varphi),$$

where $\vartheta_{i,k}$ is the starting angle of closed orbit k , $\vartheta_{f,k}$ is the returning angle, $m_{12,k}$ is the monodromy matrix element, $S_{m,k}^0$ is the classical action, α_k is the Maslov index, and δ_ℓ is the phase shift. As previously explained all classical quantities of orbits k closed at the nucleus have to be calculated with the condition that the core potential has to be switched off at the start and final return of the trajectory, as core effects related to the first and last interaction with the core are already incorporated in the semiclassical formulas via the phase shifts δ_ℓ .

In our comparison of semiclassical results with experimental spectra or exact R -matrix quantum calculations we consider dipole transitions with π -polarized light from an initial s state to final states with magnetic quantum number $m=0$. For this transition the only nonvanishing coefficient is B_{10} and we obtain

$$f^0 = 2(E_f - E_i) |B_{10}|^2,$$

$$\mathcal{Y}_0^\delta(\vartheta) = \tilde{\mathcal{Y}}_0^\delta(\vartheta) = -e^{i\delta_1} B_{10} \sqrt{\frac{3}{4\pi}} \cos\vartheta \quad (37)$$

and

$$f = f^0 \left\{ 1 + \sum_{\text{cl.o.k}} A_k \sin(S_k - \phi_k) \right\}, \quad (38)$$

with the amplitudes and phases

$$\begin{aligned} A_k = & \sqrt{18\pi \sin\vartheta_{i,k} \sin\vartheta_{f,k}/|m_{12,k}|} \cos\vartheta_{i,k} \cos\vartheta_{f,k}, \\ \phi_k = & -2\delta_1 + \frac{\pi}{2} \alpha_k - \frac{\pi}{4}. \end{aligned} \quad (39)$$

F. Recurrence spectra at constant scaled energy

A special feature of a purely hydrogenic system in a magnetic field is its scaling property with respect to the magnetic field strength. With scaled coordinates and momenta,

$$\tilde{\mathbf{r}} = \gamma^{2/3} \mathbf{r}, \quad \tilde{\mathbf{p}} = \gamma^{-1/3} \mathbf{p}$$

the classical Hamiltonian can be written in the form

$$\tilde{H} = \gamma^{-2/3} H = \frac{1}{2} \tilde{\mathbf{p}}^2 - \frac{1}{\tilde{r}} + \frac{1}{8} \tilde{\rho}^2 = \tilde{E}. \quad (40)$$

The classical trajectories obtained from the scaled equations of motion do not depend on both energy and magnetic field strength but on only one parameter, the scaled energy $\tilde{E} = E\gamma^{-2/3}$. Because the classical action scales as

$$S_k = 2\pi\tilde{S}_k\gamma^{-1/3} \quad (41)$$

(the factor of 2π is introduced for convenience only) each closed orbit k contributes a sinusoidal modulation in $\gamma^{-1/3}$ to the oscillator strength at constant scaled energy. The modulations become most transparent in the Fourier transform of photoabsorption spectra at constant scaled energy \tilde{E} . These so-called recurrence spectra exhibit sharp resonances at the positions of the scaled classical action of closed orbits; i.e., they can be interpreted semiclassically in terms of closed orbits starting at and returning to the nucleus. Varying the scaled energy \tilde{E} the bifurcation scheme of closed orbits [25] can be systematically analyzed in the recurrence spectra [8,11].

The scaling property is lost, in general, for nonhydrogenic atoms in magnetic fields because the size of the ionic core does not depend on the magnetic field strength. In our model potential (3), this loss manifests in the fact that the length parameter a determining the range of the core potential is constant and does not scale like $\tilde{a} = a\gamma^{2/3}$. But if the range of interest for the magnetic field strength γ is not too large, $a\gamma^{2/3}$ may be assumed to be constant in good approximation and is chosen to reproduce the quantum defects μ_ℓ of a given atom at the center of the interval. With this appointment the same scaling laws as for hydrogen can now be applied to nonhydrogenic atoms. Recurrence spectra at constant scaled energy are most appropriate, also for general Rydberg atoms, to perform comparisons between generic features in quantum spectra and the related classical dynamics.

Applying the scaling relation for the classical action [Eq. (41)] and for the monodromy matrix element ($\tilde{m}_{12} = m_{12}\gamma^{1/3}$) and introducing

$$z \equiv \gamma^{-1/3}$$

the oscillating part of the photoabsorption spectrum can be written as

$$f^{\text{osc}}(z) = f^0\gamma^{1/6} \sum_{\text{cl.o.},k} \tilde{A}_k \sin(2\pi\tilde{S}_k z - \phi_k).$$

The Fourier transform recurrence spectra can be calculated analytically in the approximation that $\gamma^{1/6} \approx \gamma^{1/6}$ is assumed constant in the Fourier transformed interval $[z_1, z_2]$. With $\bar{z} = 1/2(z_1 + z_2)$ and $\Delta z = z_2 - z_1$ we obtain

$$\begin{aligned} F(\tilde{S}) &= \frac{1}{\Delta z} \int_{z_1}^{z_2} f^{\text{osc}}(z) e^{2\pi i\tilde{S}(z-\bar{z})} dz \\ &= \frac{1}{\Delta z} f^0 \gamma^{1/6} \int_{z_1}^{z_2} e^{2\pi i\tilde{S}(z-\bar{z})} \sum_{\text{cl.o.},k} \tilde{A}_k \sin(2\pi\tilde{S}_k z - \phi_k) dz \\ &= f^0 \gamma^{1/6} \sum_{\text{cl.o.},k} \tilde{A}_k \frac{\sin(\pi(\tilde{S}-\tilde{S}_k)\Delta z)}{2\pi(\tilde{S}-\tilde{S}_k)\Delta z} e^{i(\phi_k - 2\pi\tilde{S}_k\bar{z} + \pi/2)}. \end{aligned} \quad (42)$$

In the case of an infinite length of the photoabsorption spectrum ($\Delta z \rightarrow \infty$) each closed orbit k contributes a δ function at

position $\tilde{S} = \tilde{S}_k$ to the recurrence spectrum (42). For finite length Δz the resonances are broadened and may overlap. In this case the complex phases in (42) ensure the correct consideration of interference effects in the calculation of recurrence strengths $F(\tilde{S})$, which are complex numbers in general. If there is no interest in the complex phase of these numbers recurrence spectra are taken as absolute value or absolute value squared of $F(\tilde{S})$.

Regarding transitions from an initial s state to final states with $m=0$ the amplitudes \tilde{A}_k and phases ϕ_k are given by Eq. (39) (with $m_{12,k}$ replaced with the scaled quantities). In this form Eq. (42) has been applied to obtain the semiclassical recurrence spectra presented in the next paragraph.

V. COMPARISON OF RECURRENCE SPECTRA

Nonhydrogenic resonance structures in recurrence spectra have been discovered in R -matrix quantum calculations of a model atom with one nonzero quantum defect ($\mu_1 \neq 0$) [13]. Similar structures have also been recently observed in experimental spectra and R -matrix calculations of helium [14]. We are now able to compare the recurrence spectra of Refs. [13] and [14] with rigorous semiclassical results and to explain the nonhydrogenic resonances in terms of families of core-scattered closed orbits.

A. Model atom at scaled energy $\tilde{E} = -0.3$

In Ref. [13] the transition from hydrogenic to nonhydrogenic spectra has been analyzed in varying the quantum defect μ_1 in R -matrix calculations between $\mu_1 = 0$ (i.e., hydrogen) and $\mu_1 = 0.9$. At scaled energy $\tilde{E} = -0.3$ the recurrence spectrum at $\mu_1 = 0.5$ [Fig. 7(b)] significantly deviates from the hydrogenic spectrum [Fig. 8(b)]: Pronounced resonances are observed, which do not appear in hydrogen and at positions where no hydrogenic closed orbits exist. One of them labeled with Y is situated at $\tilde{S} \approx 4.4$, and another at $\tilde{S} \approx 3.3$.

In our classical calculations we chose $Z = 2.269$ and $a = 1$ in the potential (3) to obtain a quantum defect of $\mu_1 = 0.5$. Because of the huge exponential proliferation of the number of closed orbits with increasing action the calculations have been restricted to $\tilde{S} < 4.8$. The semiclassical recurrence spectra are presented in Figs. 7(a) and 8(a). They show the same features as the R -matrix calculations of Ref. [13] and we are now able to explain these structures in terms of families of structural similar closed orbits.

Let us start the discussion with the resonance structure at $4.2 < \tilde{S} < 4.6$ labeled with Y in Fig. 7(b). It is built up by a superposition of several hundred core-scattered closed orbits as illustrated in Fig. 9. The figure presents the recurrence amplitudes A_k of nonhydrogenic orbits [calculated with Eq. (39)]. The cluster of strongest amplitudes around $\tilde{S} \approx 4.5$ belongs to the closed-orbit family $R_2^1 \oplus V_2^{2*}$, whereas clusters of resonances at $\tilde{S} \approx 4.3$ and $\tilde{S} \approx 4.45$ belong to the orbit families $R_3^1 \oplus V_1^1$ and $R_2^1 \oplus V_2^1$, respectively. Some members of these families are plotted in Fig. 10. In addition to the single-scattered orbits also multiple-scattered orbits contribute to the observed resonance structures. Indeed, we find any combination of double and triple core-scattered orbits of the kind $R_1 \oplus V_2^1 \oplus R_1$ or $R_1 \oplus V_1^1 \oplus R_1 \oplus V_1^1$. These multiple-

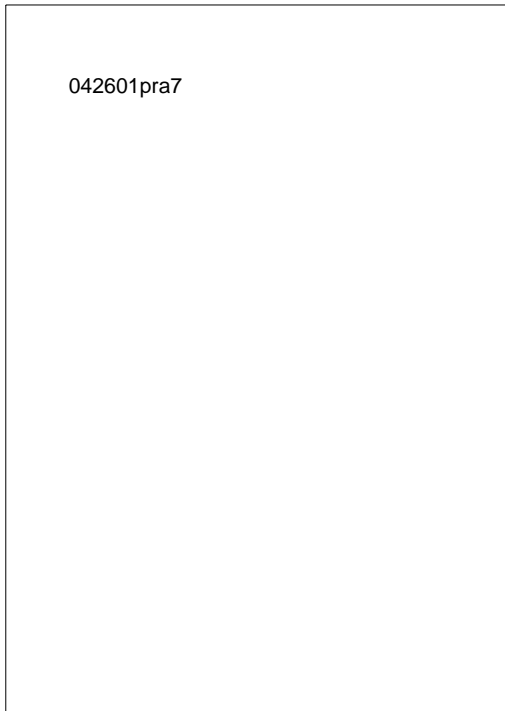


FIG. 7. Fourier transform recurrence spectra (transition to final states $m^{\pi}=0^{-}$) of a nonhydrogenic atom with quantum defect $\mu_1=0.5$. Scaled energy $\tilde{E}=-0.3$. (a) Semiclassical calculation; (b) R -matrix quantum calculation [13]. Some resonances are labeled with closed orbits or their symbolic names [8].

scattered orbits have quite a low amplitude, but of course, their total number is extremely high as any permutation of primitive hydrogenic orbits is possible and, as discussed above, every core-scattering produces a whole family of similar shaped orbits.

The resonance structure at $\tilde{S} \approx 3.3$ is easier to explain as there are fewer possibilities to build up core-scattered orbits of this quite short length from primitive hydrogenic orbits. The strongest amplitudes belong to single-scattered orbits of the family $V_1^1 \oplus R_2^1$ but there exist small contributions of double-scattered orbits $R_1 \oplus V_1^1 \oplus R_1$ as well.

B. Helium atom at scaled energy $\tilde{E} = -0.7$

Recently the helium atom was investigated experimentally with high-resolution constant scaled-energy spectroscopy [12,14]. Metastable $1s2s^3S_1$ He atoms were excited with CW laser light π polarized with respect to the magnetic field axis to final states with magnetic quantum number $m=0$. Recurrence spectra at scaled energy $\tilde{E}=-0.7$ reveal nonhydrogenic resonance structures at large actions in agreement with R -matrix quantum calculations [14]. The novel nonhydrogenic structures are marked by arrows in Figs. 11(b) and 11(c).

The p -wave quantum defect of helium close to the ionization threshold is $\mu_1=0.0684$ and all quantum defects μ_l for higher angular momenta are negligibly small. In our calculations we chose nuclear charge $Z=2$ and length parameter $a=0.33$ in the potential (3) to model the helium atom. The semiclassical recurrence spectrum is presented in Fig. 11(a). For comparison the semiclassical recurrence spectrum of hy-

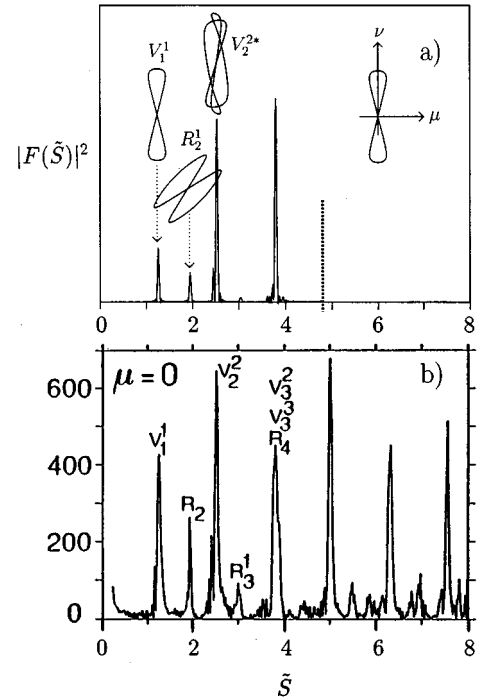


FIG. 8. Same as Fig. 7 but for the hydrogen atom, i.e., with quantum defect $\mu_1=0$.

drogen together with the quantum calculation of Ref. [14] are to be found in Fig. 12. The agreement between the semiclassical results, the experimental spectrum, and the R -matrix quantum calculations is strikingly good even for the very details in which the helium atom deviates from hydrogen [26].

We are now going to explain the novel resonance structures in helium. Experimentally two new resonances appear at scaled action $\tilde{S} \approx 10.65$ and $\tilde{S} \approx 11.45$, which can now be identified with families of core-scattered orbits: There are several possibilities to combine two or more orbits to approximately achieve these actions. In Fig. 11, we have indicated all types of double-scattered orbits that we have actually found. For illustration some graphs of orbits are drawn in Fig. 13. It is clearly visible how they are composed of two primitive hydrogenic orbits. There is even a much greater number of multiple core-scattered orbits, e.g., the orbit $R_7^1 \oplus V_7^1$ has almost the same action as $R_1 \oplus R_6^1 \oplus V_7^1$. Any combination of primitive hydrogenic orbits R_μ^v and V_μ^v existing at scaled energy $\tilde{E}=-0.7$ seems to be possible. The 13 000 most stable orbits we have used in our calculations are only a small, perhaps 1%, subset of all multiple-scattered orbits as we have estimated by an extensive closed-orbit search in a very small range of starting angles. Searching for all orbits is a difficult task with regard to a reasonable employment of computer resources. But, every additional core scattering leads to an enormous loss of recurrence amplitude and we assume that orbits scattered more than three times can be neglected in the periodic orbit sum of the semiclassical spectrum. This assumption is supported by the good quantitative agreement between the semiclassical, experimental, and R -matrix spectrum (see Fig. 11).

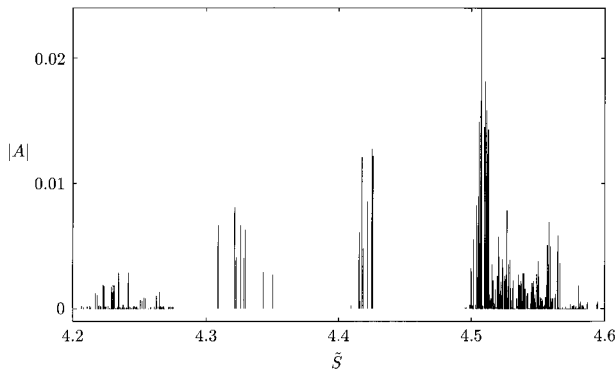


FIG. 9. Section of the amplitude spectrum at scaled energy $\tilde{E} = -0.3$ and quantum defect $\mu_1 = 0.5$. The lines represent the recurrence strength of nonhydrogenic closed orbits generating by coherent superposition the resonance structure labelled with Y in Fig. 7.

In the quantum mechanically calculated spectrum of helium [Fig. 11(c)] there appear two further resonances at $\tilde{S} \approx 9.0$ and $\tilde{S} \approx 9.8$ dominantly built up from double-scattered orbits of families $R_\mu^1 \oplus V_\nu^1$ with an index sum $\mu + \nu = 11$ and $\mu + \nu = 12$, respectively. We also find an additional resonance at $\tilde{S} \approx 8.15$, which is very weak in the quantum spectrum. The corresponding core-scattered orbit consists of two hydrogenic orbits R_5^1 and V_5^1 that do not exist at scaled action $\tilde{E} = -0.7$, but are born at slightly higher scaled energy.

VI. CONCLUSION

We have investigated nonhydrogenic Rydberg atoms in magnetic fields in a rigorous semiclassical approach. The non-Coulombic nature of the ionic core has been considered in classical trajectory calculations via a short-ranged core

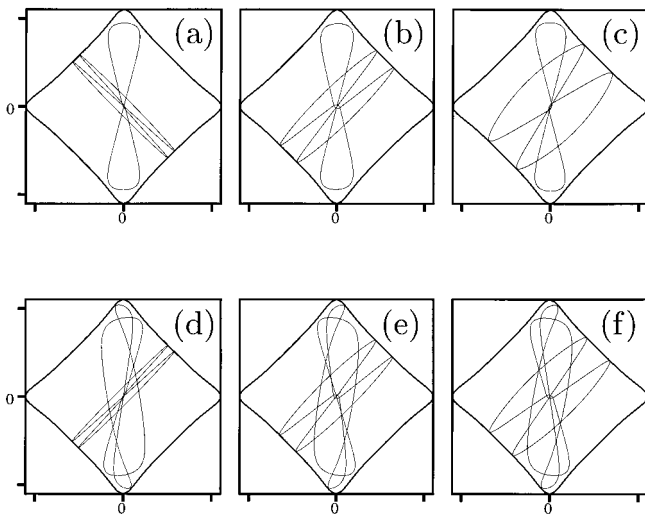


FIG. 10. Some core-scattered orbits contributing to the resonance structure labeled with Y in Fig. 7. Scaled energy $\tilde{E} = -0.3$; quantum defect $\mu_1 = 0.5$. (a) – (c) Orbits of family $R_2^2 \oplus V_2^1$; (d) – (f) Orbits of family $R_2^1 \oplus V_2^{2*}$.

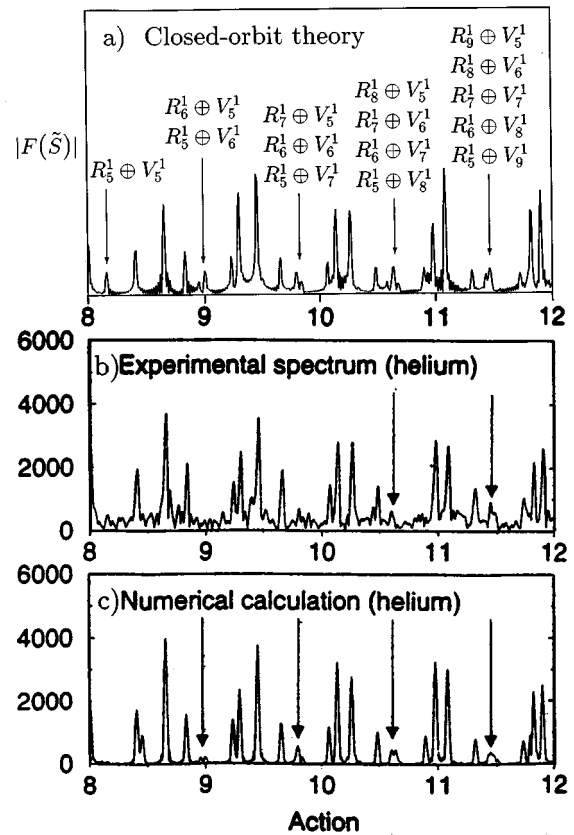


FIG. 11. Recurrence spectra of the helium atom (final states $m^{\pi} = 0^{-}$) at scaled energy $\tilde{E} = -0.7$. (a) Semiclassical calculation; (b) experimental spectrum [14]; (c) R -matrix quantum calculation [14]. Nonhydrogenic resonances are marked by arrows and labeled with families of single-scattered closed orbits.

potential and new families of core-scattered nonhydrogenic closed orbits have been discovered. With a closed-orbit theory extended to arbitrary quantum defects of the ionic core semiclassical recurrence spectra of nonhydrogenic at-

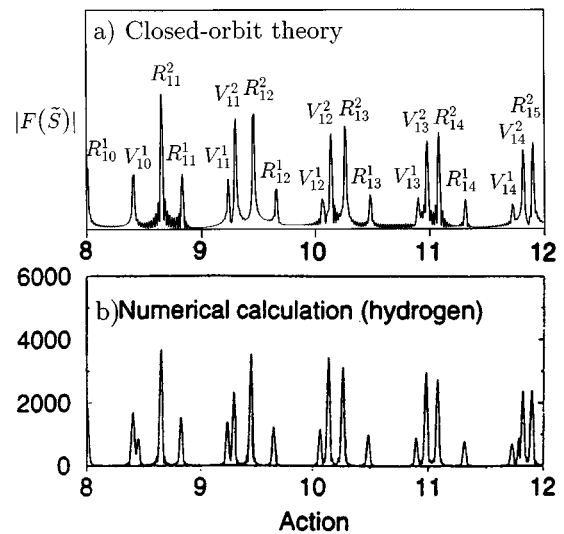


FIG. 12. Same as Fig. 11 but for the hydrogen atom. (a) Semiclassical calculation; (b) R -matrix quantum calculation [14].

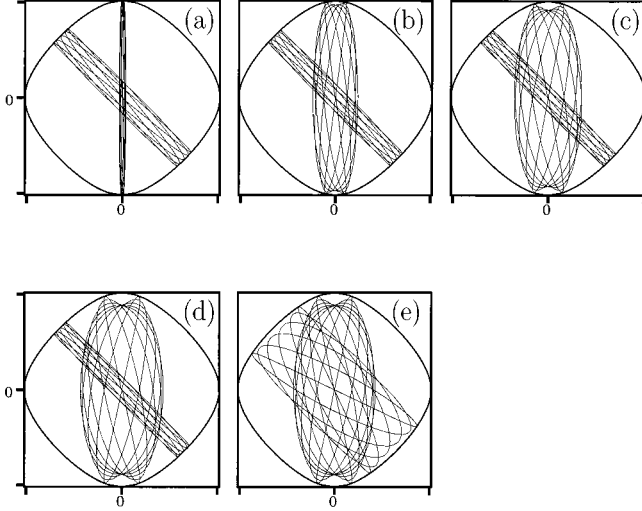


FIG. 13. Some examples of single-scattered closed orbits of the helium atom at scaled energy $\tilde{E} = -0.7$. They belong to families (a) $R_5^1 \oplus V_5^1$; (b) $R_5^1 \oplus V_6^1$; (c) $R_5^1 \oplus V_7^1$; (d) $R_5^1 \oplus V_8^1$; (e) $R_6^1 \oplus V_8^1$.

oms have been provided. They are in good quantitative agreement as well with R -matrix quantum calculations as with experimental measurements. Furthermore the rigorous semiclassical approach allows a deeper understanding and interpretation of the physics of general Rydberg atoms: The novel resonance structures in nonhydrogenic recurrence spectra have been recently denoted as effects “beyond periodic orbits,” which result from *quantum scattering* of returning waves at the ionic core [15]. We are now able to explain these features completely in terms of new families of closed orbits, i.e., via *classical* core scattering. It may be noted that the different approaches are not at all in contradiction but complement each other to finalize our physical picture of general Rydberg atoms in magnetic fields.

The semiclassical approach should be applicable not only to atoms in a magnetic field but to nonhydrogenic Stark spectra [16] and to atoms in crossed magnetic and electric fields [17] as well. But the numerical effort to search for core-scattered closed orbits will considerably increase in the case of nonparallel external magnetic and electric fields, as the classical motion of the highly excited electron is nonseparable in *three* degrees of freedom.

APPENDIX A: COMPUTATION OF QUANTUM DEFECTS

We calculate the quantum defects μ_ℓ of the ionic core due to the core potential (3) by two different methods, namely, quantum mechanically by numerical solution of Schrödinger’s equation and semiclassically by calculation of the classical action.

In quantum mechanics the regular wave functions $u_\ell(r) = rR_\ell^{\text{reg}}(r)$ at energy $E = 0$ are solutions of the radial equation

$$\left(\frac{d^2}{dr^2} - \frac{\ell(\ell+1)}{r^2} - 2V(r) \right) u_\ell(r) = 0, \quad (\text{A1})$$

with the condition $u_\ell(r) \sim r^{\ell+1}$ close to the origin. Equation (A1) is integrated numerically from the origin to the region outside the ionic core ($r > r_{\text{core}}$). The phase shift $\delta_\ell = \pi\mu_\ell$ is now obtained (modulo π) by comparison with the analytical form of the asymptotic wave function (12).

Semiclassically, $\hbar\delta_\ell$ is the difference in the classical action between the nonhydrogenic and hydrogenic radial motion starting at the turning point. As is well known $\ell(\ell+1)$ has to be replaced with $(\ell+1/2)^2$ in the semiclassical formulas to be valid for small angular quantum numbers [27]. With the hydrogenic part in Eq. (5) solved analytically, $r_0 = 1/2(\ell+1/2)^2$, and $R > r_{\text{core}}$ we obtain

$$\delta_\ell = \int_{r_{0,c}}^R \sqrt{-2V(r) - \frac{(\ell+1/2)^2}{r^2}} dr - \sqrt{8(R-r_0)} + \sqrt{8r_0} \arctan \sqrt{\frac{R-r_0}{r_0}}. \quad (\text{A2})$$

For illustration Table I presents the quantum defects μ_ℓ for the model potential (3) and various values of the nuclear charge Z and length parameter a . The quantum and semiclassical results are in good agreement especially for the largest and most important quantum defects. The agreement is a justification for a rigorous semiclassical treatment of nonhydrogenic atoms in magnetic fields, i.e., the consideration of core effects via classical scattering.

APPENDIX B: REGULARIZATION OF EQUATIONS OF MOTION

The Coulomb singularity presents an obstacle with regard to numerical integration of the equations of motion. The way out of this problem is a transformation of time $t \rightarrow \tau$ with $dt = 2r d\tau$ called regularization [28], together with a coordinate transformation to semiparabolical coordinates $\mu = \sqrt{r+z}$ and $\nu = \sqrt{r-z}$. This results in a regularized Hamiltonian

$$\mathcal{H} = \frac{1}{2}(p_\mu^2 + p_\nu^2) - E(\mu^2 + \nu^2) - (Z-1)e^{-(\mu^2 + \nu^2)/2a} \times \left(1 + \frac{\mu^2 + \nu^2}{2a} \right) + \frac{1}{8}\gamma^2\mu^2\nu^2(\mu^2 + \nu^2) = 2. \quad (\text{B1})$$

The equations of motion obtained from the Hamiltonian (B1) are free of singularities and were integrated numerically with the help of a high-order Runge-Kutta algorithm with step width control in order to fulfill the accuracy requirement in the domain of the additional core potential. Close to the nucleus where the magnetic field can be neglected and with $E \approx 0$ the Hamiltonian (B1) describes the scattering of a free motion by the short-ranged core-potential as illustrated in Fig. 1.

Because core scattering is graphically more pronounced in semiparabolical than in cylindrical coordinates in this paper all closed orbits are drawn in semiparabolical coordinates (μ, ν) .

TABLE I. Quantum mechanical and semiclassical quantum defects μ_ℓ of the model core potential.

ℓ	$Z=3a=1$		$Z=3a=2$		$Z=4a=2$	
	$\mu_\ell^{(\text{quantum})}$	$\mu_\ell^{(\text{semicl.})}$	$\mu_\ell^{(\text{quantum})}$	$\mu_\ell^{(\text{semicl.})}$	$\mu_\ell^{(\text{quantum})}$	$\mu_\ell^{(\text{semicl.})}$
0	0.9095	0.9077	1.2982	1.2963	1.7999	1.7981
1	0.7489	0.7473	1.1924	1.1896	1.6821	1.6796
2	0.3135	0.3446	0.9471	0.9449	1.4159	1.4131
3	0.0216	0.0151	0.4955	0.5073	0.9355	0.9344
4	0.0012	0.0004	0.0684	0.0626	0.1338	0.1243
5	$<10^{-4}$	$<10^{-4}$	0.0081	0.0055	0.0127	0.0085

APPENDIX C: CLASSICAL ACTION IN THE VICINITY OF THE NUCLEUS

The classical action in the vicinity of the nucleus (with the core potential switched off, the magnetic field neglected, and $E \approx 0$) is most easily calculated in semiparabolical coordinates $\mu = \sqrt{r(1 + \cos \vartheta)}$ and $\nu = \sqrt{r(1 - \cos \vartheta)}$. With the regularized momenta $p_\mu^f = -2 \cos \vartheta_f / 2$ and $p_\nu^f = -2 \sin \vartheta_f / 2$ of orbits returning with an angle ϑ_f to the field axis we obtain

$$\begin{aligned} \Delta S &= \int_{(\mu, \nu)}^{(0,0)} (p_\mu d\mu' + p_\nu d\nu') = -p_\mu^f \mu - p_\nu^f \nu \\ &= \sqrt{8r} \cos \frac{\vartheta_f - \vartheta}{2}. \end{aligned} \quad (\text{C1})$$

For $\vartheta \approx \vartheta_f$ we get the desired expression to derive Eq. (28).

APPENDIX D: CALCULATION OF THE MONODROMY MATRIX

The monodromy matrix \mathbf{M} is the stability matrix restricted to deviations perpendicular to a periodic orbit after period time T . We only discuss systems with two nonseparable degrees of freedom (like atoms in a magnetic field). If $\delta q(0)$ is a small deviation perpendicular to the orbit in coordinate space at time $t=0$ and $\delta p(0)$ an initial deviation in momentum space, the corresponding deviations at time $t=T$ are related to the monodromy matrix [10]:

$$\begin{pmatrix} \delta q(T) \\ \delta p(T) \end{pmatrix} = \mathbf{M} \begin{pmatrix} \delta q(0) \\ \delta p(0) \end{pmatrix} = \begin{pmatrix} m_{11} & m_{12} \\ m_{21} & m_{22} \end{pmatrix} \begin{pmatrix} \delta q(0) \\ \delta p(0) \end{pmatrix}. \quad (\text{D1})$$

To compute \mathbf{M} one considers an initial deviation solely in coordinate space to obtain the matrix elements m_{11} and

m_{21} , and an initial deviation solely in momentum space to obtain m_{12} and m_{22} . In practice a linearized system of differential equations obtained by differentiating Hamilton's equations of motion with respect to the phase-space coordinates is numerically integrated.

For closed orbits starting at the origin and calculated in semiparabolical coordinates (μ, ν) an initial deviation in momentum space perpendicular to the orbital motion can be expressed by a deviation in the starting angle ϑ_i

$$\begin{pmatrix} \delta p_\mu(0) \\ \delta p_\nu(0) \end{pmatrix} = \begin{pmatrix} -p_\nu(0) \\ p_\mu(0) \end{pmatrix} \frac{\delta \vartheta_i}{2}$$

and the deviations of coordinates at the final return are

$$\begin{pmatrix} \delta \mu(T) \\ \delta \nu(T) \end{pmatrix} = \begin{pmatrix} \frac{\partial \mu}{\partial \vartheta_i}(T) \\ \frac{\partial \nu}{\partial \vartheta_i}(T) \end{pmatrix} \delta \vartheta_i.$$

By projection the matrix element m_{12} is now obtained as

$$m_{12} = \frac{1}{2} \left(p_\mu(T) \frac{\partial \nu}{\partial \vartheta_i}(T) - p_\nu(T) \frac{\partial \mu}{\partial \vartheta_i}(T) \right). \quad (\text{D2})$$

If the Jacobian (26) is written in semiparabolical coordinates μ, ν and the new time τ

$$J(t, \vartheta_i) = \mu \nu \det \left| \frac{\partial(\mu, \nu)}{\partial(\tau, \vartheta_i)} \right| = r \sin \vartheta \left(p_\mu \frac{d\nu}{d\vartheta_i} - p_\nu \frac{d\mu}{d\vartheta_i} \right). \quad (\text{D3})$$

Equation (29) is derived by comparison with Eq. (D2) for the monodromy matrix element m_{12} .

[1] H. Friedrich and D. Wintgen, Phys. Rep. **183**, 37 (1989).
[2] H. Hasegawa, M. Robnik, and G. Wunner, Prog. Theor. Phys. **98**, 198 (1989).
[3] S. Watanabe, in *Review of Fundamental Processes and Applications of Atoms and Ions*, edited by C. D. Lin (World Scientific, Singapore, 1993).
[4] D. Delande, in *Chaos and Quantum Physics*, edited by M. J. Giannoni, A. Voros, and J. Zinn-Justin, Les Houches Lecture Notes, Session LII (North-Holland, Amsterdam, 1991), p. 665.

[5] W. R. S. Garton and F. S. Tomkins, Astrophys. J. **158**, 839 (1969).
[6] A. R. Edmonds, J. Phys. (Paris), Colloq. **31**, C4-71 (1970).
[7] A. Holle, G. Wiebusch, J. Main, B. Hager, H. Rottke, and K. H. Welge, Phys. Rev. Lett. **56**, 2594 (1986); J. Main, G. Wiebusch, A. Holle, and K. H. Welge, *ibid.* **57**, 2789 (1987).
[8] A. Holle, J. Main, G. Wiebusch, H. Rottke, and K. H. Welge, Phys. Rev. Lett. **61**, 161 (1988); J. Main, G. Wiebusch, and K. H. Welge, Commun. At. Mol. Phys. **25**, 233 (1991).

- [9] M. L. Du and J. B. Delos, Phys. Rev. A **38**, 1896 (1988); **38**, 1913 (1988).
- [10] E. B. Bogomol'nyi, Zh. Éksp. Teor. Fiz. **96**, 487 (1983) [Sov. Phys. JETP **69**, 275 (1989)].
- [11] J. Main, G. Wiebusch, K. Welge, J. Shaw, and J. B. Delos, Phys. Rev. A **49**, 847 (1994).
- [12] T. van der Veldt, W. Vassen, and W. Hogervorst, Europhys. Lett. **21**, 903 (1993).
- [13] T. S. Monteiro and G. Wunner, Phys. Rev. Lett. **65**, 1100 (1990).
- [14] D. Delande, K. T. Taylor, M. H. Halley, T. van der Veldt, W. Vassen, and W. Hogervorst, J. Phys. B **27**, 2771 (1994).
- [15] P. A. Dando, T. S. Monteiro, D. Delande, and K. T. Taylor, Phys. Rev. Lett. **74**, 1099 (1995).
- [16] M. Courtney, H. Jiao, N. Spellmeyer, and D. Kleppner, Phys. Rev. Lett. **73**, 1340 (1994); M. Courtney, N. Spellmeyer, H. Jiao, and D. Kleppner, Phys. Rev. A **51**, 3604 (1995).
- [17] G. Raithel, H. Held, L. Marmet, and H. Walther, J. Phys. B **27**, 2849 (1994).
- [18] J. Gao, J. B. Delos, and M. Baruch, Phys. Rev. A **46**, 1449 (1992); J. Gao and J. B. Delos, *ibid.* **46**, 1455 (1992).
- [19] B. Hüpper, J. Main, and G. Wunner, Phys. Rev. Lett. **74**, 2650 (1995).
- [20] P. A. Dando, T. S. Monteiro, W. Jans, and W. Schweizer, Prog. Theor. Phys. Suppl. **116**, 403 (1994).
- [21] H. Goldstein, *Classical Mechanics* (Addison-Wesley, Reading, MA, 1950).
- [22] P. M. Morse and H. Feshbach, *Methods of Theoretical Physics* (McGraw-Hill, New York, 1953), Pts. I and II.
- [23] V. P. Maslov and M. V. Fedoriuk, *Semiclassical Approximation in Quantum Mechanics* (Reidel, Boston, 1981).
- [24] J. B. Delos, Adv. Chem. Phys. **65**, 161 (1986).
- [25] J. M. Mao and J. B. Delos, Phys. Rev. A **45**, 1746 (1992).
- [26] In Figs. 11(a) and 12(a) the absolute value of the semiclassical recurrence strength $F(\vec{S})$ is plotted. Thereby weak nonhydrogenic resonance structures are even more pronounced than in Ref. [19] where the absolute value squared is drawn.
- [27] L. D. Landau and E. M. Lifshitz, *Quantum Mechanics* (Pergamon, New York, 1958).
- [28] E. L. Stiefel and G. Scheifele, *Linear and Regular Celestial Mechanics* (Springer, Berlin, 1971).